

Mechanics promotes coherence in heterogeneous active media

Soling Zimik¹ and Sitabhra Sinha^{1,2}

¹The Institute of Mathematical Sciences, CIT Campus, Taramani, Chennai 600113, India

²Homi Bhabha National Institute, Anushaktinagar, Mumbai 400094, India

(Dated: August 21, 2024)

Synchronization of activity among myocytes constituting vital organs, e.g., the heart, is crucial for physiological functions. Self-organized coordination in such heterogeneous ensemble of excitable and oscillatory cells is therefore of clinical importance. We show by varying the strength of intercellular coupling and the electrophysiological diversity, a wide range of collective behavior emerges including clusters of synchronized activity. Strikingly, stretch-activated currents allow waves of mechanical deformation to alter the activity of neighboring cells, promoting robust global coherence.

Cells whose contractility are mediated by electrical signals are central to many vital physiological processes [1–3]. Examples include the myocytes in the heart and smooth muscle cells in the uterus and the gastrointestinal tract [4–6]. While the mechanisms that result in changes in the electrical state of the cells (in the form of action potentials) give rise to contractions of the myofibrils - a process referred to as excitation-contraction coupling - has been investigated at great depth, the manifestation - at the tissue-scale - of communication between neighboring cells through such interacting electrical and mechanical activities is less well-understood. The problem is further compounded by the fact that most biological tissues are heterogeneous mixtures of different cell types having distinct characteristic patterns of local activity - which makes the coherence achieved by the system even more remarkable. As intercellular interactions are believed to underlie the observed system-wide synchronization of activity that is functionally crucial, e.g., as in the pumping action of the heart, it is important to arrive at a comprehensive explanation of how global coordination can be achieved by these means.

Cells responding to electromechanical signals typically possess the property of *excitability* [7–10], characterized by a nonlinear response of the transmembrane potential to electrical currents. In excitable (E) cells, this manifests as an action potential elicited by a supra-threshold stimulus. Other cells, characterized as oscillatory (O) cells, spontaneously generate periodic pulses of activity. These distinct cell types coexist in many natural settings, such as, the GI tract [11], the sino-atrial node, i.e., the natural pacemaker of the heart [12] or diseased cardiac tissue [13, 14]. Note that O cells can even represent cellular aggregates comprising excitable and passive cells (e.g., fibroblasts) coupled by gap junctions that can give rise to emergent oscillations [15, 16]. These are of relevance, e.g., in the uterus, where single, isolated cells cannot exhibit autonomous activity but sites of spontaneous activity nevertheless arise during the later stages of pregnancy to coordinate organ-wide contractions that are essential for childbirth [5]. As the relative density of such cells and the strength of their coupling can change over time, for

instance, in the embryonic heart [17, 18], in the gravid uterus [5, 19, 20], or as a result of disease-related physiological alterations [13, 21], it is essential to explicate the collective dynamics resulting from electrical and mechanical interactions between these heterogeneous cell types. In particular, one would like to understand the mechanisms that promote robust coherence of periodic activity that is crucial for the functioning of these organs and whose breakdown lead to pathological outcomes such as cardiac arrhythmia, irritable bowel syndrome or premature contractions leading to pre-term birth. A crucial piece of the puzzle that has become manifest only relatively recently is provided by the coupling between electrical excitation of a cell and the resulting mechanical contraction [9, 22]. This stress in turn affects the activation of neighboring cells via mechanosensitive pathways, e.g., by inducing stretch-activated current (I_{sac}) through specialized channels [Fig. 1 (a-b)]. Thus, a wave of excitation propagating radially outward that is initiated by a local stimulation will be preceded by a mechanical deformation (stretching) of cells anterior to the wavefront, thereby stimulating I_{sac} (and hence excitation) in these cells [Fig. 1 (c-e)].

In this paper we show that such electromechanical interactions between cells enhances oscillatory activity in the system significantly over and above the contribution from electrotonic coupling via gap junctions. Indeed, even for situations where such electrical interactions are weak, the cells can coordinate by means of the tension-induced electrical activity, resulting in the emergence of robust coherence, with almost all cells oscillating in phase. We demonstrate the key role played by mechanics in promoting synchrony in the context of electrically heterogeneous media comprising both E and O cells [16, 23–25]. As the relative density of the distinct cell types and/or the strengths of electrotonic coupling between them are varied, their collective activity exhibits transitions between a variety of spatiotemporal patterns, e.g., spatially localized clusters of excitation eventually merging to states characterized by traveling waves, ultimately leading to coherence. As these in turn can be associated with various abnormal physiological

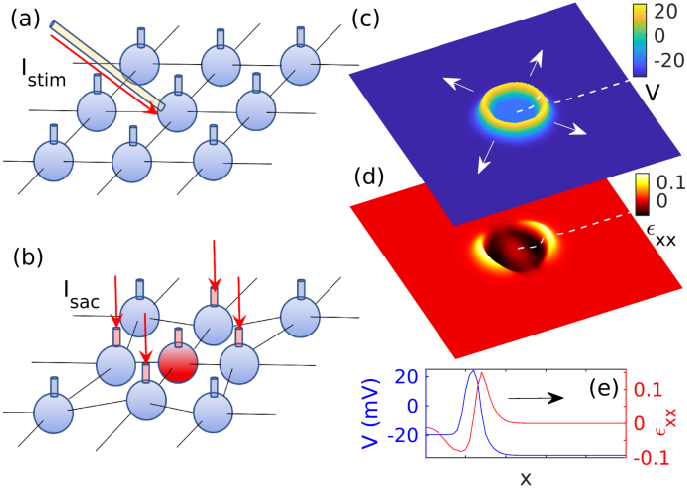


FIG. 1. Inter-cellular electromechanical coupling promotes propagation of activity across excitable media. (a-b) Excitable tissue schematically represented as a regular lattice of cells, each coupled to its neighbors both electrically and mechanically. (a) Activation of the central cell upon stimulation by current I_{stim} results in a contraction that (b) locally deforms the neighborhood and induces activity in surrounding cells by allowing current I_{sac} through their stretch-activated channels. (c-d) Point stimulation at the center of a domain results in propagation (indicated by arrows) of an excitation front in the membrane potential V (c), accompanied by a deformation manifesting as a wave in the normal strain field, whose x component, ϵ_{xx} , is shown in (d). The spatial profiles of the two waves (blue: V , red: ϵ_{xx}) along the broken line are indicated in (e). Note the deformation at locations anterior to the excitation front, moving in the direction of the arrow, that results from stretching (+ve strain) induced in its neighbors by a cell contracting (-ve strain) upon being excited.

rhythms [26, 27], our results can have potential implications of clinical relevance.

The time-evolution of the state (characterized by the transmembrane potential V) of the tissue considered as a continuum is given by

$$\partial V/\partial t = (I/C_m) + \nabla \cdot (D \nabla V) - \nabla \cdot (V \dot{\mathbf{U}}), \quad (1)$$

where C_m ($= 20 \mu\text{F cm}^{-2}$) is the membrane capacitance, and the current comprises $I = I_{bas} - I_{ion} + I_{sac}$. Here, I_{bas} is a basal current that determines whether an isolated cell is capable of spontaneous oscillations (for $I_{bas} > 90$, via a Hopf bifurcation [28]) and D is the diffusion coefficient representing the gap-junctional conductances that can vary across space. The ionic current for each cell is described according to Morris-Lecar equations [29] and comprises a K^+ current determining the recovery, a Ca^{2+} current providing the initial excitation, and a membrane leakage current, viz., $I_{ion} = g_K n(V - E_K) + g_{Ca} m_\infty (V - E_{Ca}) + g_L (V - E_L)$, where n is a gating variable for the K^+ current whose time-evolution is described by $dn/dt = (n_\infty - n)/\tau_n$. The kinetics of the Ca^{2+} channel is assumed to be relatively faster and thus,

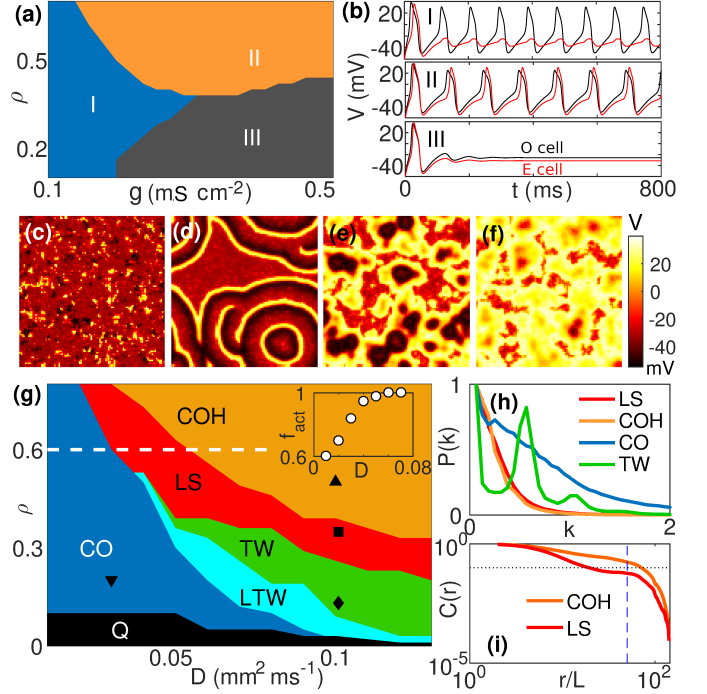


FIG. 2. Heterogeneous media, comprising excitable (E) and oscillatory (O) cells that are electrically coupled to neighbors, can display diverse spatiotemporal patterns, with coherent activity emerging only under strong coupling and for relatively higher proportion of oscillatory cells. (a-b) The collective dynamical regimes observed in the mean-field limit for different values of coupling, D , and relative fraction of O cells, ρ , correspond to: (I) O active, E inactive, (II) both O and E active, and (III) both O and E inactive [O and E are indicated by red and blue curves, respectively, in the time-series shown in (b)]. (c-f) Different spatiotemporal activity patterns observed in V for a 2-dimensional square lattice ($L = 50$) with ρ fraction of O and $(1 - \rho)$ fraction of E cells, neighbors being coupled with strength D : (c) Clustered Oscillation (CO), (d) Traveling Waves (TW), (e) Localized Synchronization (LS), and (f) Coherence (COH) [Video S1]. (g) Oscillatory activity is suppressed upon decreasing ρ , yielding Quiescent state Q. Localized Traveling Waves (LTW) regime may also be observed, in which the fraction of active cells $f_{act} < 0.9$ [Video S2]. The inset shows the variation of f_{act} with D along the broken line in the main figure to indicate the distinction between CO and LS regimes. The parameter values for the patterns in (c)-(f) are indicated using the markers ∇ , \diamond , \square and \triangle , respectively. The corresponding states can be distinguished by their (h) power spectrum $P(k)$ and (i) correlation function $C(r)$ [horizontal dotted line: $C(r) = 0.1$; vertical broken line: $r = L/2$, L being the linear extent of the domain].

the asymptotic value of $m_\infty = [1 + \tanh(V - V_1)/V_2]/2$ is used. The parameters are chosen to be $g_L = 2$, $g_{Ca} = 4.4$, $g_K = 8$ ($\text{m}\Omega \text{ cm}^{-2}$), $V_1 = -1.2$, $V_2 = 18$, $E_K = -84$, $E_{Ca} = 120$ and $E_L = -60$ (mV). The recovery of the cell after activation is governed by the K^+ current, which, in turn, is determined by the gating variable n with its asymptotic value $n_\infty = [1 + \tanh(V - V_3)/V_4]/2$

and the characteristic time $\tau_n = 25/\cosh([V - V_3]/2V_4)$, the parameters being set to $V_3 = 2$, $V_4 = 30$ [30]. The stretch-activated current $I_{sac} = g_{sac} E (V - V_{sac})$ represents the electrical contribution of mechanical interactions between the cells, with g_{sac} and V_{sac} representing conductance and reversal potential of the corresponding channel [31–33]. As stretching of the cell results in the opening of the channel [34, 35], I_{sac} is finite if the normal components of the strain ϵ are positive, measured as $E = \sqrt{\epsilon_{xx}^2 \Theta(\epsilon_{xx}) + \epsilon_{yy}^2 \Theta(\epsilon_{yy})}$, where $\epsilon_{ij} = \frac{1}{2}(\partial U_i/\partial r_j + \partial U_j/\partial r_i)$ with $\{i, j\} = \{x, y\}$, U_i are the components of the displacement vector field \mathbf{U} , \mathbf{r} is the position vector, and $\Theta(\cdot)$ is the Heaviside step function. We assume the medium to be a linear isotropic elastic solid in an overdamped environment [36, 37], such that the displacement evolves as

$$\partial \mathbf{U}/\partial t = \nabla \cdot (\boldsymbol{\sigma}^{passive} + \boldsymbol{\sigma}^{active}), \quad (2)$$

where the passive component of the stress is determined by the material properties of the solid, viz., $\sigma_{ij}^{passive} = \lambda \delta_{ij} \epsilon_{kk} + 2\mu \epsilon_{ij}$, where δ_{ij} is the Kronecker delta function and λ, μ are the Lamé parameters [38]. The active component $\sigma_{ij}^{active} = T^{active} \delta_{ij}$ results from the active tension T^{active} induced by intrinsic electrical excitation of a cell and evolves with the normalized transmembrane potential $\mathcal{V} = (V - V_{\min})/(V_{\max} - V_{\min})$, where $V_{\max} = 30$ mV and $V_{\min} = -50$ mV are the highest and lowest V values attained during an action potential] as:

$$\frac{dT^{active}}{dt} = K(\alpha \mathcal{V} - T^{active}), \quad (3)$$

where $K(\mathcal{V})$ is a function that controls the time-scale of active stress, which is defined by $K(\mathcal{V}) = 0.02(0.2)$ for $\mathcal{V} < -0.01$ ($\mathcal{V} > -0.01$) and $\alpha (= 0.3)$ controls the magnitude of the contraction impulse [39]. Thus, Eqns. (1-3) model the electromechanical coupling in the medium. The activation (rise in V) of a cell increases the tension T^{active} inside the cell, as in Eqn. (3), causing its contraction, which in turn stretches its neighboring cells and activates I_{sac} in the neighboring cells. The final (convective) term of Eqn. (1) represents the contribution to the change in potential resulting from transport due to tissue deformation.

We consider a square lattice of $L \times L$ cells ($L = 100$ for the simulations shown here, although we have verified that qualitatively similar results can be seen with other system sizes). Of these, a fraction ρ are oscillatory (O) cells capable of spontaneous periodic activation, the remaining cells being excitable (E). The former have I_{bas}^O that are randomly sampled from a uniform distribution bounded between [90, 150], while the latter are characterized by $I_{bas}^E = 70$. Each cell is coupled diffusively to its neighboring four cells in the square lattice for the simulations reported here. The diffusive coupling strength D is in general a function of space, but is taken to be a constant for most of our simulations, except those shown in

Fig. 3 (d-e), where it has a spatial gradient. The PDEs (1) and (2) are solved using a pseudospectral method [40] for the spatial part (spatial resolution $\delta x = 2$ mm) with periodic boundary conditions, while the temporal evolution of all the equations are performed by the Euler method with a temporal resolution $\delta t = 0.1$ ms. For each choice of ρ and D , results have been averaged over 10 realizations.

We begin by exploring the conditions under which the model exhibits collective dynamics characterized by various spatiotemporal activation patterns, in the absence of any mechanical interactions between the cells. To get a broad understanding of the principal regimes that are possible, we can simplify further to obtain a mean-field description of the medium in which each cell has exactly the same fraction ρ and $1 - \rho$ of O and E cells, respectively, among its k neighbors ($k = 4$ for the lattices we have shown results for). We note that such a setting will give results identical to the spatially heterogeneous situation implicit in Eqn. (1) in the limit of extremely strong gap-junctional coupling (represented by $D \rightarrow \infty$) when the system can be effectively reduced to a mutually coupled pair of O and E elements whose membrane potentials, V^O and V^E , respectively, evolve as $C_m dV^O/dt = -I_{ion} + I_{bas}^O + kg(1 - \rho)(V^E - V^O)$ and $C_m dV^E/dt = -I_{ion} + I_{bas}^E + kg\rho(V^O - V^E)$. As seen in Fig. 2 (a), in this mean-field setting, the system can be in any one of three regimes depending on the density of O cells ρ and the intercellular coupling strength g , viz., I: only the O cells show appreciable activity (for low g), II: O and E cells oscillate in phase (for high ρ and g) and III: both cells inactive (for low ρ but high g). These regimes can be intuitively understood as follows: in regime I, the coupling is too weak for the O cells (that exhibit spontaneous activity) to drive the E cells above their threshold - a situation that is rectified upon making the coupling stronger (regime II). However, if the density of O cells is relatively low (regime III), increased coupling leads to a source-sink imbalance such that the gap-junctional current from O cells is shared between too many inactive cells and is insufficient to drive any of the cells over the threshold, resulting in both cell types becoming quiescent.

Collective dynamics analogous to these three regimes can be observed even upon introducing spatial heterogeneity in the domain by randomly choosing the fraction of oscillatory neighbors of a cell from a distribution having a mean value of ρ . Thus, the clustered oscillations (CO) state obtained in the limit of weak coupling [Fig. 2 (c)], in which the O cells are active but are unable to drive all the E cells because of the low value of D , is analogous to Regime I in Fig. 2 (a). Note though that the heterogeneity introduces a degree of variability absent in the mean-field case, viz., instead of only the O cells being active at low D , activity is seen across small spatial clusters that locally have a high density of

O cells. Increasing the coupling strength results in differential outcomes depending on ρ . For a low density of O cells, this leads to cells becoming quiescent (Q) because of source-sink mismatch, analogous to the situation for regime III in the mean-field limit. As ρ is increased, the relatively strong coupling between cells imply that local clusters having a higher density of O cells act as organizing centers for activity spreading through the domain in the form of traveling waves [TW, Fig. 2 (d)]. As ρ is increased further, we observe successively larger regions of the domain getting synchronized in their activity in the locally synchronized (LS) regime [Fig. 2 (e)], eventually leading to coherence [COH, Fig. 2 (f)], such that the periodic activity of cells across the entire domain is occurring in phase, analogous to regime II in the mean-field limit.

The various types of collective dynamics discussed above arise under different conditions of cellular heterogeneity [quantifiable as $\sim \rho(1 - \rho)$] and coupling, as seen from the position of the corresponding domains in ρ - D parameter space shown in Fig. 2 (g). The inset shows the variation with D in the order parameter f_{act} , i.e., the fraction of cells undergoing persistent oscillations, for maximal heterogeneity in the cellular composition of the domain ($\rho = 0.5$). A transition from CO to LS can be observed when f_{act} exceeds 90% around $D \sim 0.03$. As already mentioned, if the relative density of O cells are decreased, then depending on the coupling strength between cells, we will either see a transition to Q (when $f_{act} < 0.1$) or TW. The latter pattern is of particular relevance for systems such as the sino-atrial node or uterine tissue where they have been observed [26, 41] and associated with aberrant functioning [27, 42]. The TW regime can be identified by the presence of a characteristic wavelength in the resulting patterns, resulting in a prominent secondary peak [Fig. 2 (h)] in the power spectrum $P(k)$ ($= \tilde{V}_k \tilde{V}_k^*$, where $\tilde{V}_k, \tilde{V}_k^*$ are the amplitudes of the k^{th} Fourier mode of $V(r)$ and its complex conjugate). If we decrease the density of O cells, the waves are eventually confined within spatially disjoint patches ($0.1 < f_{act} < 0.9$), which we refer to as *Localized Traveling Waves* (LTW) [Video S2].

As reported above, in the strong coupling regime, increasing the fraction of O cells results in the clusters exhibiting spontaneous activity becoming larger in size. The increased degree of synchronization seen as the system traverses through the LS and COH regimes with increasing ρ is reflected in the reduced width of the distribution of mode amplitudes $P(k)$ [Fig. 2 (h)]. This suggests that activity in the system is coordinated over larger length scales (corresponding to small k), which is shown explicitly by measuring the spatial correlation function $C(r) = \langle V(r_0)V(r_0+r) \rangle - \langle V(r_0) \rangle^2 / (\langle V(r_0)^2 \rangle - \langle V(r_0) \rangle^2)$ between the activity at a pair of locations separated by a distance r , the averaging being over both r_0 and time. The COH regime is distinguished from LS by the cor-

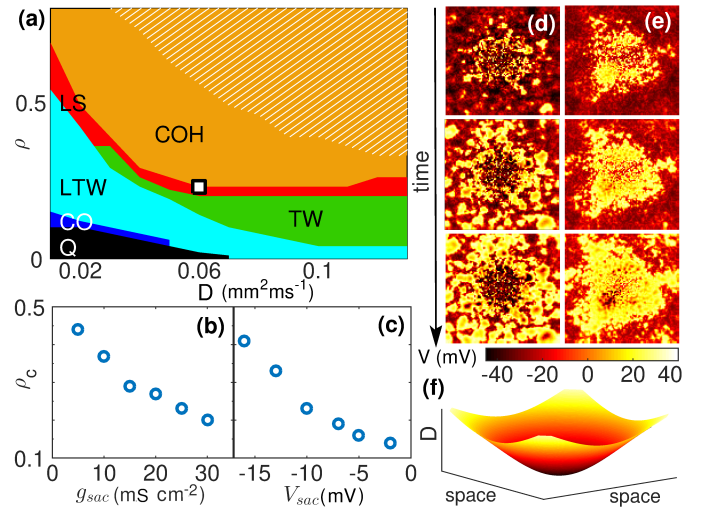


FIG. 3. Mechanical interactions promote synchronization of activity even for extremely weak electrical coupling between cells. (a) In presence of I_{sac} ($g_{sac} = 25$, $V_{sac} = -10$), coherence (COH) is observed over a much broader range of parameters ρ and D [for comparison, the hatched region shows its extent in the absence of I_{sac} , see Fig. 2 (g)]. The other globally oscillating states ($f_{act} > 0.9$), LS and TW, have extended into the regions that was occupied by the quiescent regime Q and the partially oscillatory CO domain when $g_{sac} = 0$ [see Fig. 2 (g)]. The critical value ρ_c of oscillator density at which COH emerges for $D = 0.06$ is indicated (open square). (b-c) Variation of ρ_c as a function of the conductance g_{sac} [$V_{sac} = -10$] (b) and reversal potential V_{sac} [$g_{sac} = 25$] (c) of the stretch activated channel, respectively, implying that coherence can be achieved using relatively fewer O cells by increasing either of these channel parameters. (d-e) Snapshots indicating the spatiotemporal evolution of V (time increasing from top to bottom) for $g_{sac} = 0$ (d) and 25 (e), respectively. The spatially changing strength of electrical gap-junction couplings is modeled by D varying along a gradient between $[0, 0.07]$, increasing radially from the center (f). Comparing (e) with (d), we note that the activity becomes more coherent (particularly in the central region) in the presence of mechanical interactions [Video S3].

relation length ξ over which $C(r)$ decreases to 10% of its maximum value [Fig. 2 (i)]. COH is characterized by $\xi \geq L/2$ (L being the system size), implying that almost all points in the medium are correlated.

On introducing the contribution of mechanical interactions between cells to the electrical activity via I_{sac} , which is modulated by tissue deformation (see above), we observe that synchronization is promoted in the system. This is evident from the expanded region in the ρ - D parameter space corresponding to COH [Fig. 3 (a)] in comparison to Fig 2 (a), as well as, the occurrence of LS, TW and LTW even with extremely weak gap-junctional coupling. The stretch-activated current results in the system being capable of spontaneous periodic activity over almost the entire parameter space, indicated by the significant shrinking of CO and Q. The role of the stretch

activated channel parameters, specifically, g_{sac} and V_{sac} , in driving COH can be seen from the decrease in the critical value ρ_c , the minimum relative density of O cells with which coherence can be achieved (for $D = 0.06$), as the channel conductance and reversal potential are increased, respectively [Fig. 3 (b-c)].

Mechanical interactions between the cells can also enhance synchronization in tissue where the electrical coupling displays spatial heterogeneity, e.g., a spatial gradient in the effective gap-junction conductance as has been reported in biological excitable systems such as the sino-atrial node in the heart [43, 44]. Figs. 3 (d-e) compares the spatiotemporal evolution of activity in the absence and presence, respectively, of mechanical interactions, in a medium where the electrical coupling D between cells increases radially from the center [as shown in Fig. 3 (f)]. At each cycle of periodic excitation, the activity begins in the central region that has the weakest coupling which promotes stimulation by reducing source-sink mismatch between O and E cells. Without the stretch-activated current, however, as this activity spreads outward from the center it gets fragmented because the low density of gap junctions prevent many of the cells from getting excited simultaneously [Fig. 3 (d)]. The introduction of I_{sac} provides an alternative mechanism by which cells can excite their neighbors, resulting in a more coherent pattern of spreading activity [Fig. 3 (e) and Video S3].

To conclude, we show that mechanical interactions between cells can work in tandem with electrical intercellular communication via gap junctions to create a robust mechanism for promoting synchronized oscillations in heterogeneous cell assemblies. Indeed, in the limit of weak electrotonic coupling, communication mediated by the physical deformation induced by excitation could be the primary means of coordinating collective behavior of cellular arrays. Our results are consistent with, and may help explain, recent experiments reporting the crucial role that mechanical interactions play in coordinating activity, e.g., in the embryonic heart [45]. Our observation of diverse spatiotemporal patterns can be of relevance in understanding emergent collective dynamics in media where ρ and D can vary across space (forming a gradient, as that of gap-junctional density in the sino-atrial node [43, 44]) and/or in time under natural or pathological settings (such as, the changes observed in the developing embryonic heart [17, 18], the gravid uterus [5, 19, 20] and progressively fibrotic cardiac tissue [13, 21]). The coherence enhancing mechanism described here is based on a very generic model, suggesting that it may be valid for a broad class of systems [6, 10, 41, 46]. Thus our results may provide insights about the mechanisms underlying coordination of collective activity - and hence, understanding pathologies associated with its breakdown - in heterogeneous tissue comprising excitable and oscillatory cells, as in the sino-atrial node, the gastro-intestinal tract and the gravid uterus.

SZ has been supported by the Center of Excellence in Complex Systems and Data Science, funded by the Department of Atomic Energy, Government of India. We would like thank Shakti N Menon for helpful suggestions.

-
- [1] D. Bers, *Nature (London)* **415**, 198 (2002).
 - [2] P. Langton, S. M. Ward, A. Carl, M. A. Norell and K. M. Sanders, *Proc. Natl. Acad. Sci. USA* **86**, 7280 (1989).
 - [3] H. Zheng, B. T. Drumm, S. Earley, T. S. Sung, S. D. Koh, and K. M. Sanders, *Sci. Signal.* **11**, eaaq0918 (2018).
 - [4] E. R. Pfeiffer, J. R. Tangney, J. H. Omens, and A. D. McCulloch, *J. Biomech. Eng.* **136**, 0210071 (2014).
 - [5] R. C. Young, *Reproduction* **152**, R51 (2016).
 - [6] J. D. Huizinga and W. J. Lammers, *Am. J. Physiol.-Gastr. L.* **296**, G1 (2009).
 - [7] E. Meron, *Phys. Rep.* **218**, 1 (1992).
 - [8] S. Sinha and S. Sridhar, *Patterns in Excitable Media: Genesis, dynamics, and control* (CRC Press, Boca Raton, FL, 2014).
 - [9] I. Nitsan, S. Drori, Y. E. Lewis, S. Cohen, and S. Tzllil, *Nat. Phys.* **12**, 472 (2016).
 - [10] B. Z. Jia, Y. Qi, J. D. Wong-Campos, S. G. Megason, and A. E. Cohen, *Nature (London)* **622**, 149 (2023).
 - [11] K. M. Sanders, L. F. Santana, and S. A. Baker, *J. Physiol.*, in press (2023).
 - [12] P. Camelliti, C. R. Green, I. LeGrice, and P. Kohl, *Circ. Res.* **94**, 828 (2004).
 - [13] T. P. Nguyen, Z. Qu, and J. N. Weiss, *J. Mol. Cell. Cardiol.* **70**, 83 (2014).
 - [14] Y. Okabe, N. Murakoshi, N. Kurebayashi, H. Inoue, Y. Ito, T. Murayama, C. Miyoshi, H. Funato, K. Ishii, D. Xu, and K. Tajiri, *Proc. Natl. Acad. Sci. USA* **121**, e2218204121 (2024).
 - [15] V. Jacquemet, *Phys. Rev. E* **74**, 011908 (2006).
 - [16] R. Singh, J. Xu, N. G. Garnier, A. Pumir, and S. Sinha, *Phys. Rev. Lett.* **108**, 068102 (2012).
 - [17] M. Watanabe, A. M. Rollins, L. Polo-Parada, P. Ma, S. Gu, and M. W. Jenkins, *J. Cardiovasc. Dev. Dis.* **3**, 10 (2016).
 - [18] S. R. Coppen, R. A. Kaba, D. Halliday, E. Dupont, J. N. Skepper, S. Elneil, and N. J. Severs, *Mol. Cell. Biochem.* **242**, 121 (2003).
 - [19] J. A. Lenhart, P. L. Ryan, K. M. Ohleth, and C. A. Bagnell, *Biol. Reprod.* **61**, 1452 (1999).
 - [20] B. Risek and N. B. Gilula, *Development* **113**, 165 (1991).
 - [21] N. J. Severs, S. R. Coppen, E. Dupont, H.-I. Yeh, Y.-S. Ko, and T. Matsushita, *Cardiovasc. Res.* **62**, 368 (2004).
 - [22] L. D. Weise and A. V. Panfilov, *Phys. Rev. Lett.* **108**, 228104 (2012).
 - [23] G. Bub, A. Shrier, and L. Glass, *Phys. Rev. Lett.* **88**, 058101 (2002).
 - [24] G. Bub, A. Shrier, and L. Glass, *Phys. Rev. Lett.* **94**, 028105 (2005).
 - [25] A. Kryukov, V. Petrov, L. Averyanova, G. Osipov, W. Chen, O. Drugova, and C. Chan, *Chaos* **18**, 037129 (2008).
 - [26] A. V. Glukhov, L. T. Hage, B. J. Hansen, A. Pedraza-Toscano, P. Vargas-Pinto, R. L. Hamlin, R. Weiss, C. A. Carnes, G. E. Billman, and V. V. Fedorov, *Circ. - Arrhythmia Elec.* **6**, 984 (2013).

- [27] S. R. Kharche, E. Vigmond, I. R. Efimov, and H. Dobrzynski, PLoS ONE **12**, e0183727 (2017).
- [28] K. Tsumoto, H. Kitajima, T. Yoshinaga, K. Aihara, and H. Kawakami, Neurocomputing **69**, 293 (2006).
- [29] C. Morris and H. Lecar, Biophys. J. **35**, 193 (1981).
- [30] G. B. Ermentrout and D. H. Terman, *Mathematical Foundations of Neuroscience* (Springer, New York, NY, 2010).
- [31] N. H. Kuijpers, H. M. ten Eikelder, P. H. Bovendeerd, S. Verheule, T. Arts, and P. A. Hilbers, Am. J. Physiol. - Heart C. **292**, H2832 (2007).
- [32] L. D. Weise and A. V. Panfilov, Phys. Rev. Lett. **119**, 108101 (2017).
- [33] We note that other mechanosensory mechanisms not involving a stretch-activated current have also been proposed to coordinate synchronized activity in cardiac cells, e.g., see Ref. [9].
- [34] A. Simon-Chica, A. Klesen, R. Emig, A. Chan, J. Greiner, D. Gr'un, A. Lothar, I. Hilgendorf, E. A. Rog-Zielinska, U. Ravens, P. Kohl, F. Schneider-Warme, and R. Peyronnet, J. Physiol. , in press (2024).
- [35] A. Reed, P. Kohl, and R. Peyronnet, Glob. Cardiol. Sci. Pract. **2014**, 19 (2014).
- [36] J. Yuval and S. A. Safran, Phys. Rev. E **87**, 042703 (2013).
- [37] In general, biological tissue are anisotropic [see C. Cherubini, S. Filippi, A. Gizzi, and R. Ruiz-Baier, J. Theor. Biol. **430**, 221 (2017)] but the qualitative features of the patterns reported here are not crucially dependent on this simplifying assumption of isotropy.
- [38] The numerical values for the Lamé parameters used in the simulations reported here are $\lambda = \mu = 0.4 \text{ kg mm}^{-1} \text{ ms}^{-2}$.
- [39] M. P. Nash and A. V. Panfilov, Prog. Biophys. Mol. Biol. **85**, 501 (2004).
- [40] C. Canuto, M. Y. Hussaini, A. Quarteroni, and T. A. Zang, *Spectral Methods in Fluid Dynamics* (Springer, Berlin, 1988).
- [41] W. J. Lammers, H. Mirghani, B. Stephen, S. Dhanasekaran, A. Wahab, M. A. Al Sultan, and F. Abazer, Am. J. Physiol. - Reg. I. **294**, R919 (2008).
- [42] J. Xu, S. N. Menon, R. Singh, N. B. Garnier, S. Sinha, and A. Pumir, PLoS ONE **10**, e0118443 (2015).
- [43] E. E. Verheijck, M. J. van Kempen, M. Veereschild, J. Lurvink, H. J. Jongasma, and L. N. Bouman, Cardiovasc. Res. **52**, 40 (2001).
- [44] H. Honjo, M. R. Boyett, S. R. Coppen, Y. Takagishi, T. Opthof, N. J. Severs, and I. Kodama, Cardiovasc. Res. **53**, 89 (2002).
- [45] K. K. Chiou, J. W. Rocks, C. Y. Chen, S. Cho, K. E. Merkus, A. Rajaratnam, P. Robison, M. Tewari, K. Vogel, S. F. Majkut, *et al.*, Proc. Natl. Acad. Sci. USA **113**, 8939 (2016).
- [46] R. Manchanda, S. Appukuttan, and M. Padmakumar, J. Exp. Neurosci. **13**, 1 (2019)

SUPPLEMENTARY INFORMATION

Mechanics promotes coherence in heterogeneous active media

Soling Zimik and Sitabhra Sinha

LIST OF SUPPLEMENTARY MOVIES

1. Video S1: Time-evolution of activation patterns for the different dynamical regimes: (top left) Clustered Oscillation or CO, (top right) Traveling Waves or TW, (bottom left) Localized Synchronization or LS, and (bottom right) Coherence or COH.
2. Video S2: Spatial localization of traveling waves (TW regime) at relatively low density ρ of oscillating cells and low intercellular coupling strength D .
3. Video S3: Mechanics enhances synchronization as can be observed by comparing the spatiotemporal evolution of activity V in a medium having a spatial gradient in the intercellular coupling strength D with the minimum at the center of the domain [see Fig. 3 (f) in main text]. In absence of mechanical interactions, the activity is disordered in the central region where D is lowest (left panel), while incorporating mechanics results in a high degree of synchronized activity (right panel).